Highly nonlinear dynamics in a slowly sedimenting colloidal gel

G. Brambilla,[1] S. Buzzaccaro,[2] R. Piazza,[2] L. Berthier,[1] and L. Cipelletti[1]

[1] *Université Montpellier 2, Laboratoire Charles Coulomb UMR 5221, F-34095, Montpellier, France*
CNRS, Laboratoire Charles Coulomb UMR 5221, F-34095, Montpellier, France
[2] *Dipartimento di Chimica, Politecnico di Milano, 20131 Milano, Italy*

(Dated: August 17, 2021)

We use a combination of original light scattering techniques and particles with unique optical properties to investigate the behavior of suspensions of attractive colloids under gravitational stress, following over time the concentration profile, the velocity profile, and the microscopic dynamics. During the compression regime, the sedimentation velocity grows nearly linearly with height, implying that the gel settling may be fully described by a (time-dependent) strain rate. We find that the microscopic dynamics exhibit remarkable scaling properties when time is normalized by strain rate, showing that the gel microscopic restructuring is dominated by its macroscopic deformation.

PACS numbers: 47.57.ef, 64.70.pv, 82.70.Dd

Gels and attractive glasses resulting from the aggregation of colloidal particles are the subject of extensive studies because their physical behavior often results from a complex interplay between equilibrium thermodynamics and nonequibrium dynamic processes [1–3], and because they are relevant for understanding network-forming biological systems [4] and for industrial applications. Although they exhibit solid-like mechanical properties, colloidal gels are easily disrupted by small perturbations, such as gravitational forces. While a large body of macroscopic observations of gels under gravitational stress exists [5–13], very little is known on the microscopic processes at play during sedimentation, thus limiting our ability to understand and predict the behavior of sedimenting gels.

Here, we use a novel light scattering method to gain access to the dynamics of a slowly settling colloidal system from the macroscopic deformation of the sample down to the relaxational behavior at the particle scale. We find that the very slow macroscopic deformation occurs via irreversible plastic events at the microscopic scale. Remarkably, the gel behavior at all scales is controlled by a single parameter, the time-dependent compression rate, in striking analogy with recent observations on deformed polymer [14] and colloidal [15] glasses.

We study gels formed by attractive colloidal hard spheres with radius $R = 82 \pm 3$ nm, suspended in an aqueous solvent at an initial volume fraction $\varphi_0 = 0.123$ (more details can be found in [16–18]). Gelation is induced by attractive depletion forces obtained by adding micelles of a nonionic surfactant. The interaction between colloids is well described by the Asakura-Oosawa depletion potential [16], with a range $r \approx 3$ nm. The potential can be mapped on the Adhesive Hard Sphere model, with a stickiness parameter $\tau \simeq 0.01$ [16, 17]. The density mismatch between the particles and the solvent is $\Delta\rho = 1.12$ g/cm^3. The particles have an intrinsic optical anisotropy; accordingly, they scatter light with polarization both parallel and perpendicular ("depolarized") to that of the incident radiation. The depolarized scattered intensity is an accurate probe of the local particle concentration [16].

To probe the sedimentation process in great detail, we use a custom-designed light scattering apparatus [19], sketched in Fig. SM1 [18]. A low magnification image of the sample illuminated by a vertical laser sheet of thickness 200 μm is formed onto a CCD sensor, using depolarized light scattered at $\theta = 90°$. By averaging the CCD signal over horizontal rows of pixels, we are able to measure accurately the time, t, and height, z, dependence of the volume fraction, $\varphi(z,t)$, with a spatial resolution of about 100 μm. We obtain the evolution of the local sedimentation velocity profiles, $v(z,t)$, using an Image Correlation Velocimetry (ICV) algorithm [20] that we apply to rectangular Regions Of Interest (ROIs) of the CCD images corresponding to the width of the sample and a height $\Delta z = 0.5$ mm. To quantify the microscopic dynamics, we measure space and time-resolved intensity correlation functions (ICFs)[19],

$$g_2(z,t,\tau) - 1 = \frac{< I_p(t) I_p(t+\tau) >_z}{< I_p(t) >_z < I_p(t+\tau) >_z} - 1 \,,$$

where $< \cdots >_z$ is an average over all pixels belonging to a ROI at height z. Using a mixed spatio-temporal correlation method to be described elsewhere, we correct the ICFs for the drift due to sedimentation, so that $g_2 - 1$ measures the average microscopic particle motion between times t and $t + \tau$ in the co-sedimenting frame where $v = 0$. Because we detect the depolarized scattered light, $g_2 - 1$ is proportional to the square of the self part of the dynamic structure factor, $f_s(z, \mathbf{q}, t, \tau) = N^{-1} \sum_j \exp[-i\mathbf{q}\cdot(\mathbf{r}_j(t+\tau) - \mathbf{r}_j(t))]$, where the sum is over the N particles in a ROI at height z and $\mathbf{q}$ is the scattering vector. A full decay of the ICF indicates particle rearrangements over a lengthscale $q^{-1} = 0.66R$. Thus, we are able to measure simultaneously and with both temporal and spatial resolution the local volume fraction, sedimentation velocity and microscopic relaxation

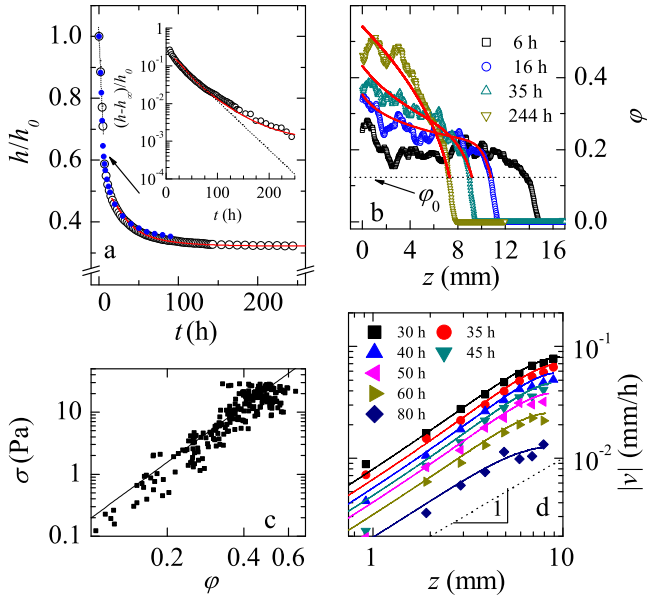

FIG. 1: (color online) (a) Temporal evolution of the normalized height of the gel, h/h_0, for cells of section 3×3 mm^2 (open circles) and 5×5 mm^2 (blue dots). The arrow shows the approximate time when the gel is formed. The solid line is the prediction of the poroelastic model, Eq. (1). Inset: reduced height vs. t in a semilog plot. The dotted line is an exponential fit to the initial decay of the reduced height, the line is the fit of the poroelastic model. (b) Concentration profiles for various times, as shown by the labels. The lines are fits of the poroelastic model. (c) $\sigma(\varphi)$ obtained experimentally by integrating the asymptotic concentration profile ($t = 244$ h). The line is the power law σ[Pa] $= 197\varphi^3$. (d) Double logarithmic plot of the velocity profiles $v(z)$ (symbols, labeled by time), together with predictions from the poroelastic model (solid lines).

dynamics, in contrast to previous works were only the total gel height, $h(t)$ [6, 7, 10–12], or at most $\varphi(z,t)$ [9, 21] could be measured.

Figure 1 illustrates the time dependence of $h(t)$, $\varphi(z,t)$, and $v(z,t)$, where $z = 0$ is the cell bottom. Up to $t \approx 6$ h, the sample is partitioned in a supernatant with $\varphi \approx 0$ at the top, an intermediate region with $\varphi = \varphi_0$, and a denser cake that builds up from the bottom. Rapid fluctuations of the scattered intensity indicate that the intermediate region is formed by disconnected falling clusters, while fluctuations are much slower in the bottom part, revealing that a gel has formed. After ≈ 6 h, a relatively loose gel ($\varphi \lesssim 0.25$, Fig. 1b) occupies the entire colloid-rich phase. We follow the slow compaction of the gel over more than 10 days, during which its height relaxes asymptotically towards a plateau $h_\infty \approx 7.3$ mm. While the time evolution of $h(t)$ may be fitted by an exponential decay at short times [11–13], deviations are clearly observed over days (inset of Fig. 1a), suggesting that sedimentation is controlled by a distribution of relaxation times, well reproduced [22] by the poroelastic model discussed below. The total strain of the gel is about 50%, such that the gel sediments at an extremely small average strain rate of order $\dot\epsilon \approx 10^{-6}\mathrm{s}^{-1}$. As shown in Fig. 1b, this very slow macroscopic deformation corresponds to a nontrivial inhomogeneous evolution of the local volume fraction $\varphi(z,t)$: $\varphi(z = h(t), t) \approx \varphi_0$ at all times, while at the bottom φ increases up to $\varphi(z = 0) \approx 0.5$.

We now turn to the behavior of the local sedimentation velocity, a quantity not accessible in previous work. Surprisingly, the large volume fraction inhomogeneity has no effect on $v(z,t)$, which grows linearly with z at all times except for the uppermost layer, see Fig. 1d. This behavior suggests to characterize the sedimentation with a single time-dependent parameter, the strain rate $\dot\epsilon = \mathrm{d}v/\mathrm{d}z$, a remarkable, but highly nontrivial simplification.

Our detailed set of measurements allows us to perform a rigorous quantitative test of the modeling of gels as a "poroelastic" medium pioneered by Buscall and White [5] and used in several studies [11–13, 21]. The modeling simplifies in the absence of wall friction. Our velocimetry analysis indicates that there is no horizontal component of the displacement resulting from the compression of the gel, i.e. that the (effective) Poisson ratio of the gel is negligible, a remarkable property that was discussed before [11] but could not be measured experimentally. Accordingly, no significant fraction of the gravitational stress is redirected on the walls, making wall friction vanish, as suggested also by the observation that changing the cell section from 3×3 mm^2 to 5×5 mm^2 does not change the evolution of h, φ, v nor that of the microscopic dynamics discussed below. Neglecting inertial terms, by balancing the gravitational stress on a gel slice by the sum of the viscous stress, due to the flow of the suspending fluid through the network, and the restoring stress resulting from the gel response to a deformation, one gets [5, 23]:

$$\frac{\partial\varphi}{\partial t} = \frac{\partial}{\partial z}\left[\frac{\varphi\kappa(\varphi)}{\eta}\left(\Delta\rho\varphi g + \frac{K(\varphi)}{\varphi}\frac{\partial\varphi}{\partial z}\right)\right], \qquad (1)$$

where $K(\varphi) = \varphi\partial\sigma/\partial\varphi$ is the effective compressional modulus in response to an applied stress σ, and $\kappa(\varphi)$ is the gel permeability, a constant on the order of the typical pore cross section that relates the solvent flow rate to the pressure drop in Darcy's law; η and g are the solvent viscosity and the gravitational acceleration, respectively. The boundary conditions are $\varphi(z = h, t) = \varphi_0$ and zero mass flux at the cell bottom. The initial conditions are obtained from the concentration and velocity profiles measured experimentally at $t = 16$ h.

The solution of Eq. (1) depends crucially on the material properties via $\kappa(\varphi)$ and $K(\varphi)$. The compressional modulus may be estimated from the concentration profile at large t, when $v \approx 0$ [13, 17]. For $t \to \infty$, the viscous stress vanishes and the restoring stress $\sigma[\varphi(z)]$ at a given height balances the total weight per unit area of the particles lying above. Thus, a numerical integration of the

equilibrium profile along z yields $\sigma(\varphi)$ [13, 17]. As shown in Fig. 1c, this yield stress is well fitted by $\sigma = a\varphi^{3\pm0.3}$, where the exponent is close to that measured for the φ dependence of the linear elastic shear modulus of colloidal gels with short-ranged interactions [24].

Various forms have been proposed in the past for the permeability $\kappa(\varphi)$, but no stringent tests on the validity of the competing expressions could be performed, owing to the lack of detailed measurements of the sedimentation kinetics. Expressions assuming a fractal morphology of the gel [11] fail to reproduce our data, presumably because the volume fraction of our gel is too large for a fully fractal structure to develop. Instead, we find that $\kappa(\varphi) = \kappa_0 \frac{(1-\varphi)^m}{\varphi}$, as in Ref. [25], reproduces very well the behavior of $h(t)$, see Fig. 1a. The fitting parameters are $\kappa_0 = 6.78 \times 10^{-2}$ μm^2, corresponding to a typical pore size in the range $0.4R - 5.9R$ (depending on φ), and $m = 7$, slightly higher that $m = 5.5 - 6.5$ typically reported for hard spheres [23, 25]. With κ_0 and m fixed by the fit to $h(t)$, Eq. (1) is solved to obtain the temporal evolution of the full concentration and velocity profiles. Remarkably, we find that the poroelastic model captures very well –with no further adjustable parameters– both $\varphi(z,t)$ and $v(z,t)$, as shown in Figs. 1b and 1d, demonstrating its efficient modeling of the sedimentation kinetics of our gel at both macroscopic and mesoscopic scales, and suggesting that the sedimentation occurs slow enough for the effective compressional modulus to approach its asymptotic limit at $\dot{\epsilon} \to 0$.

Although very successful, the poroelastic model provides no insight on the microscopic dynamics and its relation with the macroscopic deformation, a key issue unexplored so far. Given that $K(\varphi)$ appears to be unaffected by the settling kinetics, one wonders whether the microscopic dynamics of the gel is also independent of sedimentation. Indeed, it has been argued that gravitational compaction provides a convenient way to slowly change φ in order to probe the equilibrium dynamics of attractive colloidal systems as a function of particle concentration [26], implicitly assuming that microscopic dynamics and sedimentation decouple.

To investigate the link between microscopic rearrangements and the macroscopic gel compaction, we examine the intensity correlation functions $g_2(z,t,\tau)-1$. Figure 2 shows $g_2 - 1$ for several heights and times during the gel sedimentation. At all t, a full decay of $g_2 - 1$ is observed, indicating that the microstructure is continuously changing. At large t, an intermediate plateau becomes increasingly visible and $g_2 - 1$ exhibits a two-step decay. We report in Fig. 2b the decay time of the final relaxation of the ICF, $\tau_{1/e}$, defined by $g_2(\tau_{1/e}) - 1 = e^{-1}[g_2(\tau = 1\text{ s}) - 1]$. At any given time, $\tau_{1/e}$ is nearly independent of z. Thus, the microscopic dynamics is fairly homogeneous across the sample, in striking contrast with the highly inhomogeneous concentration profiles reported in Fig. 1b. While

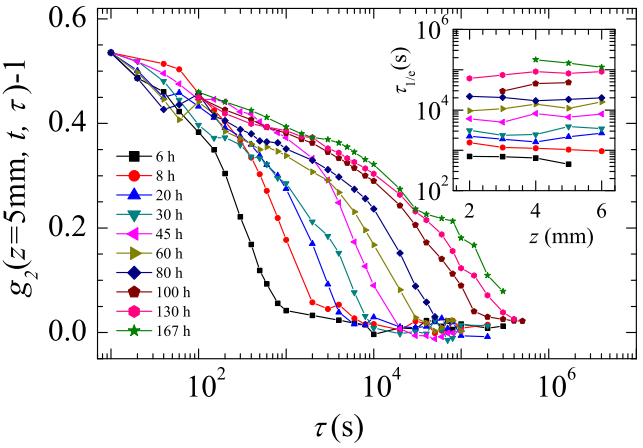

FIG. 2: (color online) Main panel: intensity autocorrelation function measured at different sedimentation times as indicated by the labels, for a cell of section 3×3 mm^2. To avoid overcrowding the graph, we plot only data for a representative height, $z = 5$ mm. Inset: relaxation time $\tau_{1/e}$ as a function of height z for various times (same symbols as in the main plot). For all times, $\tau_{1/e}$ does not depend on z.

volume fraction usually controls the spontaneous dynamics occurring in attractive gels and glasses [1, 2], we conclude that φ plays no such direct role in our system. Similarly, $\tau_{1/e}$ is independent of $v_{\rm rel} = v/(1-\varphi)$, the fluid velocity relative to the particles, because $v_{\rm rel}$ grows with z (data not shown) while $\tau_{1/e}$ is z-independent. This rules out the possibility [6] that the dynamics is due to rearrangements induced by the flow of solvent through the gel structure. This is further substantiated by the fact that the strain rate associated with the gel deformation ($\dot{\epsilon} \lesssim 10^{-5}$ s^{-1}, see Fig. 3) is at least two orders of magnitude smaller than that sustained without flow-induced damage by gels in typical linear rheology experiments. Finally, the decay of $g_2 - 1$ cannot be due to the relative motion of particles imposed by the affine vertical compression of the gel, since the ICF is sensitive only to the horizontal component of the displacement, parallel to $\mathbf{q}$.

Instead, we suggest that structural reorganization is in fact a highly nonlinear process induced by the very small, but finite, strain rate $\dot{\epsilon}$ of the sedimenting gel. In colloidal [15], polymeric [14] and molecular [27] glasses under stress, the microscopic dynamics is unaffected by the flow when the inverse strain rate is much larger than the equilibrium structural relaxation time. Because the latter can become very large in amorphous materials, very small rates can enhance particle mobility, to the point where the macroscopic flow rate controls the microscopic relaxation time. To test this hypothesis, we plot in Fig. 3 $\tau_{1/e}$ *vs.* the measured strain rate $\dot{\epsilon}$. The data are very well fitted by a power law, $\tau_{1/e} \sim \dot{\epsilon}^{-0.98\pm0.02}$ over more than two orders of magnitude, establishing a direct relationship between microscopic structural relaxation and macroscopic flow, $\tau_{1/e} \sim \dot{\epsilon}^{-1}$, analogous to that observed

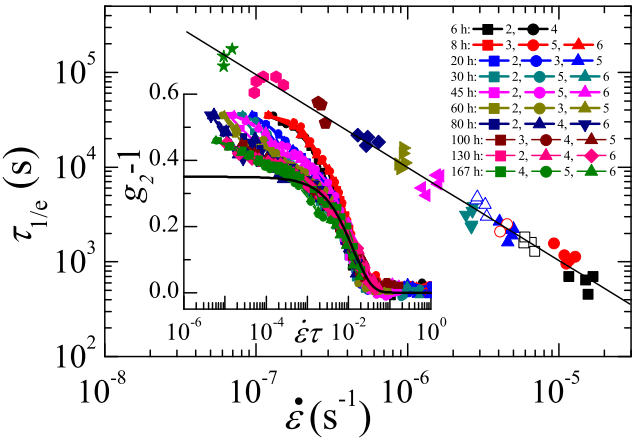

FIG. 3: (color online) Main panel: double logarithmic plot of $\tau_{1/e}$ *vs.* $\dot{\epsilon}$. Solid line: power law fit yielding $\tau_{1/e} \sim \dot{\epsilon}^{-0.98\pm0.02}$. The solid symbols are as in Fig. 2, the open symbols are data for a cell of section 5×5 mm^2 and time $t = 18, 25$, and 30 h for squares, circles and triangles, respectively. Inset: scaling of $g_2 - 1$ measured at various heights and times (see labels, where height is in mm), when plotted against $\dot{\epsilon}\tau$. The line is the function $0.35\exp(-75\dot{\epsilon}\tau)$.

in strongly sheared glassy materials. As a further test, we plot in the inset of Fig. 3 $g_2 - 1$ against rescaled time $\dot{\epsilon}\tau$. Although the initial decay of $g_2 - 1$ varies with t, the second step of the relaxation of the ICFs measured at different heights and times collapses reasonably well onto a master curve (line). Note that structural rearrangement due to plastic events occurs for a cumulated strain $\dot{\epsilon}\tau_{1/e}$ of the order of 1%, comparable to typical yield strains measured in colloidal systems [15] or molecular glass formers [28, 29].

Our experiments provide direct evidence that in a colloidal gel sedimenting over several days, the small external perturbation induced by gravitational forces has dramatic consequences at the particle scale, where structural relaxation continuously occurs at a rate imposed by the macroscopic deformation of the sample, in striking analogy with the enhancement of particle mobility observed in deformed repulsive colloidal glasses [15] and polymeric glasses [14]. Given the intricate and non-linear nature of the microscopic dynamics, it is all the more remarkable that the simple macroscopic poroelastic model widely used in sedimentation and filtration problems can successfully describe the sedimentation kinetics of our gel to a remarkable accuracy, by specifying only a couple of effective mechanical properties of the material.

We gratefully acknowledge funding from Région Languedoc Roussillon, ANR "Dynhet", CNES, Institut Universitaire de France, and the Italian Ministry of University and Research (MIUR) (PRIN 2008). We thank Solvay-Solexis (Bollate, Italy) for providing us with the colloidal particles.

[1] L. Cipelletti and L. Ramos, J. Phys.: Condens. Matter **17**, R253 (2005).
[2] E. Zaccarelli, J. Phys.: Condens. Matter **19**, 323101 (2007).
[3] C. P. Royall, S. R. Williams, T. Ohtsuka, and H. Tanaka, Nature Materials **7**, 556 (2008).
[4] K. E. Kasza, A. C. Rowat, J. Y. Liu, T. E. Angelini, C. P. Brangwynne, G. H. Koenderink, and D. A. Weitz, Curr. Opin. Cell Biol. **19**, 101 (2007).
[5] R. Buscall and L. R. White, J. Chem. Soc., Faraday Trans. **83**, 873 (1987), part 3.
[6] C. Allain, M. Cloitre, and M. Wafra, Phys. Rev. Lett. **74**, 1478 (1995).
[7] D. Senis and C. Allain, Phys. Rev. E **55**, 7797 (1997).
[8] W. C. K. Poon *et al.*, Faraday Discuss. **112**, 143 (1999).
[9] L. Stars *et al.*, J. Phys.: Condens. Matter **14**, 2485 (2002).
[10] C. Derec, D. Senis, L. Talini, and C. Allain, Phys. Rev. E **67**, 062401 (2003).
[11] S. Manley, J. M. Skotheim, L. Mahadevan, and D. A. Weitz, Phys. Rev. Lett. **94**, 218302 (2005).
[12] J. M. Condre, C. Ligoure, and L. Cipelletti, J Stat Mech - Theory and Experiments p. P02010 (2007).
[13] C. Kim, Y. Liu, A. Kuhnle, S. Hess, S. Viereck, T. Danner, L. Mahadevan, and D. A. Weitz, Phys. Rev. Lett. **99**, 028303 (2007).
[14] H. N. Lee, K. Paeng, S. F. Swallen, and M. D. Ediger, Science **323**, 231 (2009).
[15] R. Besseling, E. R. Weeks, A. B. Schofield, and W. C. K. Poon, Phys. Rev. Lett. **99**, 028301 (2007).
[16] S. Buzzaccaro, R. Piazza, J. Colombo, and A. Parola, J. Chem. Phys. **132**, 124902 (2010).
[17] S. Buzzaccaro, R. Rusconi, and R. Piazza, Phys. Rev. Lett. **99**, 098301(2007).
[18] See EPAPS Document No. XXXXXXXXXXXX for a supplementary figure and sample details. For more information on EPAPS, see http:/www.aip.org/pubservs/epaps.html.
[19] A. Duri, D. A. Sessoms, V. Trappe, and L. Cipelletti, Phys. Rev. Lett. **102**, 085702 (2009).
[20] P. T. Tokumaru and P. E. Dimotakis, Exp. Fluids **19**, 1 (1995).
[21] J. J. Lietor-Santos, C. Kim, P. Lu, A. Fernandez-Nieves, and D. Weitz, Eur. Phys. J. E **28**, 159 (2009).
[22] S. P. Usher, P. J. Scales, and L. R. White, AIChe J. **52**, 986 (2006).
[23] R. Buscall, Colloids and Surfaces **43**, 33 (1990).
[24] T. Gisler, R. C. Ball, and D. A. Weitz, Phys. Rev. Lett. **82**, 1064 (1999).
[25] J. F. Richardson and W. N. Zaki, Trans. Inst. Chem. Eng **32**, 35 (1954).
[26] Y. Gao and M. L. Kilfoil, Phys. Rev. Lett. **99**, 078301 (2007).
[27] L. Berthier and J.-L. Barrat, J. Chem. Phys. **116**, 6228 (2002).
[28] R. A. Riggleman, H. N. Lee, M. D. Ediger, and J. J. de Pablo, Phys. Rev. Lett. **99**, 215501 (2007).
[29] K. Miyazaki, D. R. Reichman, and R. Yamamoto, Phys. Rev. E **70**, 011501 (2004).